ENVIRONMENTAL STUDIES

Human disturbances dominated the unprecedentedly high frequency of Yellow River flood over the last millennium

Shi-Yong Yu[1]*, Wen-Jia Li[2,3], Liang Zhou[1], Xuefeng Yu[4], Qiang Zhang[5,6], Zhixiong Shen[7]

A warming climate may increase flood hazard through boosting the global hydrological cycle. However, human impact through modifications to the river and its catchment is not well quantified. Here, we show a 12,000-year-long record of Yellow River flood events by synthesizing sedimentary and documentary data of levee overtops and breaches. Our result reveals that flood events in the Yellow River basin became almost an order of magnitude more frequent during the last millennium than the middle Holocene and 81 ± 6% of the increased flood frequency can be ascribed to anthropogenic disturbances. Our findings not only shed light on the long-term dynamics of flood hazards in this world's most sediment-laden river but also inform policy of sustainable management of large rivers under anthropogenic stress elsewhere.

INTRODUCTION

River floods represent a transient response of the fluvial system to excessive discharge, which is of great societal relevance, particularly to riparian communities. A deep understanding of the long-term dynamics of river floods is of overwhelming importance not only for developing strategies and measures for preparedness, adaptation, and disaster management but also for improving the prediction of future changes in flood frequency. It has been shown that intensifying hydrological cycle attributed to a warming climate may push up flood hazards in most rivers of the world (1, 2). However, the impact of human disturbances to river systems on flood hazards remains obscure (3). Given that the proportion of the global population exposed to floods is increasing (4), it is urgent to bridge this knowledge gap to improve flood risk prediction.

In addition to the socioeconomic impacts, river floods also represent an active morphodynamical agent, playing an important role in shaping the hydromorphic landscape of Earth. Large rivers and their floodplains are also birthlands of human civilizations. In the absence of remarkable human interferences, continental-scale fluvial systems have been regulated by the combined internal processes and external climate changes and tectonics during geological episodes. However, from the last century onward, most of the world's major rivers and their basins began to be modified by anthropogenic disturbances such as deforestation, channelization, embankment, and dam construction in an unprecedented pace to meet the increasing needs for flood control, power generation, agricultural irrigation, and commercial navigation (5), gradually evolving into a coupled human-natural system. Despite the societal benefits, existing evidence from the Rhine and Mississippi rivers suggests that river embankment may raise the base flow, thereby amplifying the climate-mediated flood magnitude (6–8). Yet, this paradox of flood enhancement through flood control was not well evidenced in other large rivers at a longer time scale.

The Yellow River basin (Fig. 1) is a cultural landscape with an indelible imprint of human interventions during the CE (9). Upstream erosion and downstream embankment continuously raised the riverbed, eventually giving rise to an 800-km-long confined and superelevated channel belt perching around 10 m above the surrounding ground in the lower reaches of the river (10). Such a perched river system was highly unstable, marked by frequent levee breaches and channel avulsions (11). Documentary records show that the lower Yellow River changed its course on 26 occasions from 602 BCE to 1949 CE (12, 13), of which six are most prominent (Fig. 1). Therefore, the Yellow River presents an exceptional opportunity to disentangle impacts of human disturbances and climate changes on flood hazards for a continental-scale river system. Here, we seek to understand the long-term dynamics of Yellow River flood events and place them within a context of human-environment interactions. We found that flood events in the Yellow River basin became much more frequent during the last millennium than the middle Holocene mostly due to the enhanced human disturbances on the river and its basin. Meanwhile, our modeling results indicated that proactive soil and water conservation on the Loess Plateau was critical for flood mitigation downstream.

RESULTS

We reconstruct the frequency of Yellow River flood events associated with levee overtops and breaches during the last 12,000 years through a rigorous synthesis and analysis of multisource data (Supplementary Text). Historical and modern flood events during the last 3000 years are based on levee breaches and overtops described meticulously in various official documents (tables S1 to S6). We compile these events according to several criteria, and the timeline of these events is presented in Fig. 2A. Usually occurring in the

[1]School of Geography, Geomatics and Planning, Jiangsu Normal University, Xuzhou 221116, China. [2]Group of Alpine Paleoecology and Human Adaptation (ALPHA), State Key Laboratory of Tibetan Plateau Earth System, Resources and Environment (TPESRE), Institute of Tibetan Plateau Research, Chinese Academy of Science, Beijing 100101, China. [3]University of Chinese Academy of Sciences, Beijing 100049, China. [4]State Key Laboratory of Loess and Quaternary Geology, Institute of Earth Environment, Chinese Academy of Sciences, Xi'an 710075, China. [5]Advanced Interdisciplinary Institute of Environment and Ecology, Beijing Normal University, Zhuhai 519087, China. [6]Faculty of Geographical Science, Beijing Normal University, Beijing 100875, China. [7]Department of Marine Science, Coastal Carolina University, Conway, SC 29526, USA.
*Corresponding author. Email: syu@jsnu.edu.cn
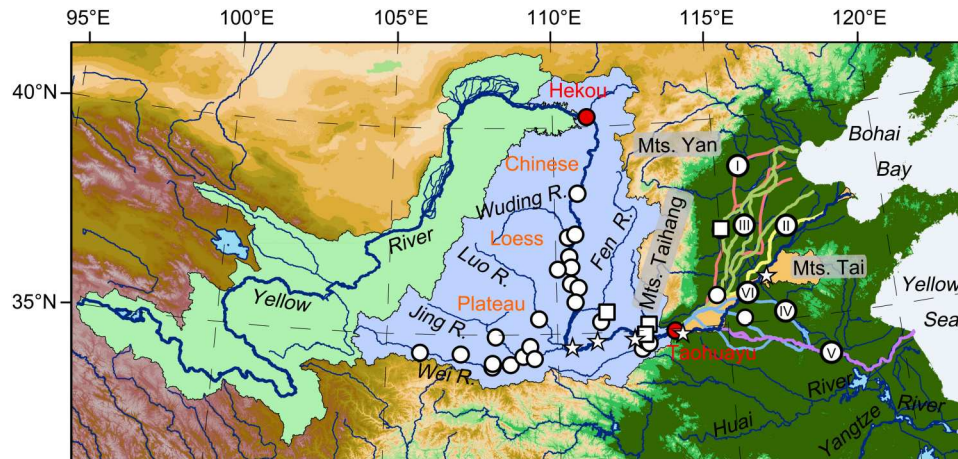
Fig. 1. Map showing the topographical feature of the Yellow River watershed. Filled dots and squares denote the location of optically stimulated luminescence (OSL)– and radiocarbon (^{14}C)–dated paleo-flood slack water deposits, respectively. Stars aligned from west to east indicate the Shanxian, Xiaolangdi, Huayuankou, and Sunkou gauging stations, respectively. Major river stages are as follows: I, 602 BCE to 11 CE; II, 11 to 1048 CE; III, 1048 to 1128 CE; IV, 1128 to 1368 CE; V, 1368 to 1855 CE; and VI, 1855 CE to present.

aftermath of excessive rainfall in the summer, levee breaches and overtops exhibit remarkable spatial variability on the lower Yellow River and its floodways (fig. S1). Paleo-flood events are based on 137 slack water deposits preserved in the context of loess-paleosol sequences and/or archaeological cultural strata (tables S7 and S8), among which 112 were dated directly using optically stimulated luminescence (OSL) and 25 were dated using radiocarbon (^{14}C) (fig. S2). Unlike those buried underneath the floodplain, elevated slack water deposits in the middle Yellow River basin provide a conservative estimate of paleo-flood peak stage and discharge of the main stream (*14*).

The sedimentary data have built-in error arising from dating uncertainty, which may have more or less impact on the calculation of flood frequency. To deal with temporal uncertainties in the sedimentary data, a hierarchical Bayesian model was developed to infer the true ages of paleo-flood events (Materials and Methods). A total of 1000 uncorrelated timelines of paleo-flood events were obtained using the Markov chain Monte Carlo (MCMC) method (Fig. 2B). To evaluate the performance of our age model, we calculate the posterior mean and 95% confidence interval of the modeled ages and plot them against the laboratory ages for comparison (fig. S3). The data points fall well on the 1:1 line, indicating that the modeled and laboratory ages are nearly equal to one another. Note that dated slack water deposits are scarce after ca. 1000 BCE. A comparison with historical leave failures suggests that such a scarcity of sedimentary data is actually a reflection of research bias against younger flood events.

To accommodate the propagation of dating error in the sedimentary record when calculating flood frequency, we bootstrap the less error-prone documentary records for 1000 times as well through random sampling with replacement. The bootstrapped mean ages of historical and modern flood events also well correlate to their calendar ages (fig. S4), indicating the robustness of our approach to tackling temporal uncertainties in the data. Note that uncertainties in the bootstrapped ages are generally small (2 to 10 years), while large errors may occur particularly in the periods that data are relatively scarce (e.g., before 500 CE). These

uncertainties will be transferred to the equivalent uncertainty in the calculated flood frequency. We merge the modeled paleo-flood events to the bootstrapped historical and modern flood events, forming a suite of long flood timelines, each of which was then used to calculate flood frequency in terms of occurrence rate using a Gaussian kernel (Materials and Methods).

Our flood record, particularly the sedimentary paleo-flood record, may have been subject to more or less taphonomic bias (fig. S5). Using an empirical model derived from a large dataset of global volcanic deposits (*15*), we correct our flood record for taphonomic bias (Materials and Methods). Clearly, taphonomic bias has a remarkable impact on the calculated flood frequency, particularly for the early time period (fig. S6). The taphonomically corrected record of flood frequency exhibits considerable variations superimposed on a significantly (Cox-Stuart test, $P < 0.0001$) increasing trend (Fig. 2C). Mean flood occurrence rate was as low as ca. 0.04 year^{-1} during 10,000 to 5000 BCE, indicating a flood-poor period. After a period of progressive decrease to almost 0.02 year^{-1}, flood frequency increased by an order of magnitude from 3500 to 1000 BCE. Subsequently, mean flood frequency fluctuated below 0.1 year^{-1} and then turned to increase monotonically from 500 CE. Mean flood occurrence rate reached ca. 0.4 year^{-1} by 1000 CE, marking the onset of an unprecedently flood-rich period.

DISCUSSION
We ascribe the long-term increase of Yellow River flood frequency over the last 12,000 years to the progressively enhanced human-environment interactions, particularly on the Loess Plateau, the world's largest landmass of aeolian sediments characterized today by fragmented topography and enlarged altitudinal gradients. Given that the Loess Plateau is both the major water and sediment sources of the lower Yellow River (*16*), scrutinizing human-environment interactions on this fragile landscape is essential for identifying the driving forces of long-term variability of Yellow River flood frequency. We compile and analyze a variety of geological and archaeological records, which were generally classified as
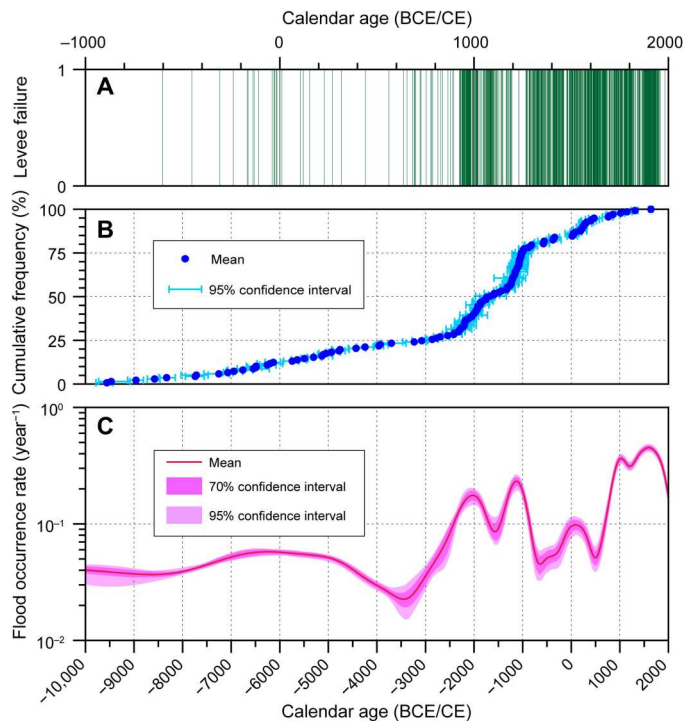
Fig. 2. Reconstruction of Yellow River flood frequency during the last 12,000 years. (**A**) Documentary record of levee beaches and overtops. (**B**) Modeled calendar ages of paleo-flood slack water deposits. (**C**) Gaussian kernel density estimation of flood occurrence rate.

natural drivers [e.g., relative sea-level changes in the Bohai Bay (*17*), annual precipitation (*18*), vegetation cover of gully areas (*19*), and soil development (*20*)], anthropogenic drivers [e.g., expansion of millet-based agriculture and Neolithic settlement (*21*), introduction of domesticates characterizing the steppe culture (*22*), and technological innovations such as water well construction (*23*), coal mining (*24*), copper smelting (*25*), cast iron technology (*26*), and embankment (*27*)], and responses of the fluvial system [flood frequency, sediment yield (*28*), and channel aggradation rate (*29*)]. The longue durée of human-environmental interactions under the evolving climate and geomorphic boundary conditions during the Holocene can be roughly divided into four phases (fig. S7).

The first phase (10,000 to 5000 BCE) represents the climate-dominated condition with negligible human impacts. The low sea level preconditioned the lower Yellow River a downcutting valley characterized by extremely low sediment yields. Under the optimal climate condition for vegetation and soil development (fig. S7A), fluvial flood events were rare. The second phase (5000 to 2500 BCE) marks the transition from a climate-dominated to a human-dominated system (*30*, *31*). Local sea level approached the present-day position, marking the onset of an aggrading channel (fig. S7B). Millet-based agriculture began to expand onto the Loess Plateau, but it had only localized impact on the landscape. The third phase (2500 to 500 BCE) is characterized by rapidly enhancing human disturbances. Millet-based agriculture was well established, and steppe cultural elements such as bread wheat, sheep/goat, and cattle were introduced to this area (fig. S7C). Human disturbances such as coal mining and copper smelting began to exert

impacts on the system (*24*, *25*), resulting in two episodes of relatively high flood frequency. Fluvial floods clustering around 2000 BCE may have resulted from the 4.2-ka (thousand year) cold event (*32*, *33*), while those around 1100 BCE might be a key factor of frequent capital relocations in China's Central Plain during the Shang Dynasty (*34*). The fourth phase (500 BCE to 2000 CE) represents a dominance of anthropogenic influences over climate on the system. Artificial levees began to be constructed from the Western Han Dynasty (202 BCE to 9 CE) to prevent occasional flooding, gradually transforming the lower Yellow River from a freely meandering channel to a confined channel. Note that flood frequency was relatively low and the river maintained its course for hundreds of years during the first millennium CE largely due to the increased vegetation cover, while the Loess Plateau was occupied by the nomadic people (*9*). Climate continued to shift toward accelerated aridity during the last millennium, coupled with enhancing agricultural practices in wheat farming and expanding technological innovations notably in cast iron production, thereby leading to the emergence of the gully landscape (*30*). Driven by the increasing population pressure and expanding use of coal and iron tools in the Northern Song Dynasty (960 to 1121 CE) (*35*), the farming-pastoral ecotone has greatly shifted northward (*36*). Forests were cleared to put more lands under cultivation (*37*), leading to a surge of soil erosion (*38*). A total of four major avulsions occurred during this period (Fig. 1).

Our above analyses demonstrate that the natural and anthropogenic factors have combined to create some environmental effects, which gradually pushed the fluvial system into a state characterized by more frequent flood hazards and channel avulsions during the last millennium than ever. To quantify the natural and anthropogenic effects on the substantially increased flood frequency during the last millennium, we conduct an attribution analysis using multiple linear regression (Materials and Methods). To deal with the collinearity of the explanatory variables, principal components analysis (PCA) was performed (fig. S8). The time period of 5000 to 2500 BCE was chosen as the baseline, because the geomorphic boundary condition (sea level) was similar to that of today and human impacts were minimal. Data covering the baseline period were used to train and validate the regression model (fig. S9). Once optimal model parameters were obtained (table S9), we predict the changes in flood frequency under natural conditions only since 5000 BCE (Fig. 3A). Compared with the baseline condition (0.04 ± 0.01 year^{-1}), flood frequency during the last millennium increased by 0.32 ± 0.07 year^{-1} (Fig. 3B). The predicted increase caused by natural factors is only 0.06 ± 0.02 year^{-1}, accounting for ca. $19 \pm 6\%$ of the overall increases in the flood frequency. Subtracting the predicted value from the observed values yields a contribution of 0.26 ± 0.06 year^{-1} from the anthropogenic factors, implying that ca. $81 \pm 6\%$ of the increased flood frequency is caused by human modifications to the river and its basin. This value is very close to the proportion of human-induced soil erosion over the Loess Plateau (*28*) but slightly higher than that caused by river embankment in the lower Mississippi River (*8*).

Scrutinizing the interactions and feedback pathways of the natural and anthropogenic factors in the fluvial system may deepen our understanding about the dynamics of flood hazards (fig. S10). Land exposure and soil erosion are two physical processes in the socioecological system of the Loess Plateau (*39*), which are causally interrelated and reinforced one another through a positive
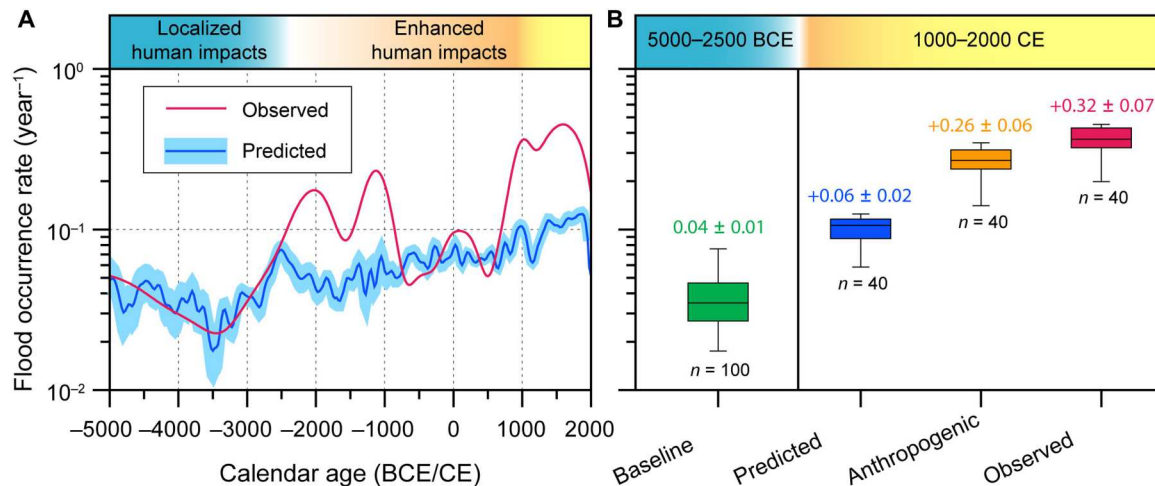
Fig. 3. Attribution of the increased flood frequency during the last millennium. (**A**) Changes in the observed flood frequency compared with that predicted from a regression model using only natural factors. (**B**) Comparison of the observed flood frequency during the baseline period (green boxplot) with that predicted from a regression model using only natural factors (blue boxplot) and observed (red boxplot) during the last millennium. Anthropogenic contribution (orange boxplot) was inferred by subtracting the predicted from the observed values.

feedback loop (9). As erosion increases, vegetation becomes more difficult to recover, and more bare areas are created, which, in turn, further exacerbates erosion. The environmental effect of erosion is then propagated and amplified iteratively in the lower Yellow River by a sequence of positive feedback loops. Embankment plays a pivotal role in these reinforcing processes. As channel aggradation proceeds, if artificial levees were constructed for flood control, the base flow of the river and the superelevation between the riverbed and the surrounding flood basin would be increased accordingly (40), thereby resulting in a situation where massive floods with an increasing magnitude and frequency occur inevitably (8). As large floods become frequent, more embankments are needed, which, in turn, cause more silt to accumulate within the channel. Therefore, humans' propensity of flood control through embankment always instigates a paradox (41). Note that the link from soil erosion to channel aggradation is positive, while the link from channel aggradation to soil erosion is negative, forming a balancing (negative feedback) loop. However, this process is too weak to maintain the equilibrium of the fluvial system under increasing anthropogenic stress (42), eventually pushing it to evolve into a perched channel belt with frequent flood hazards and channel avulsions.

On the basis of the above analyses, we model flood frequency changes during the CE using a minimalistic differential equation consisting of intrinsic growth and external harvesting (Materials and Methods), which were parameterized with the time-varying sediment yield (Fig. 4A) and embankment frequency (Fig. 4B), respectively. The good agreement of the modeled and observed flood frequency suggests that this model can capture the fundamental dynamics of flood hazard of the fluvial system (Fig. 4C). Using the optimal estimation of model parameters, a bifurcation analysis was performed to study the steady-state behavior of the fluvial system in response to external perturbations (Materials and Methods). For example, in the absence of embankment, the system has three unstable equilibria at 0, 2.0, and 3.0 Gt/year, respectively (Fig. 4D). It could still remain in a stable state with low

flood frequencies as sediment yield increases but remains less than 3.0 Gt/year (e.g., the first millennium CE). However, once sediment yield crosses this tipping point, the system would suddenly jump to another stable state characterized by high flood frequencies through a fold bifurcation. Conversely, in the case of frequent embankment (e.g., once a year), the two nontrivial fixed points annihilate each other, and the system has only one unstable equilibrium at 0 Gt/year (Fig. 4D), where a transcritical bifurcation occurs. In this case, the system is extremely sensitive to the changes in sediment yield—a slight increase in sediment yield could result in a much large increase in flood frequency (e.g., the last millennium CE). The amplification of flood frequency by embankment can also be illustrated by examining the steady-state nonlinear response of the system under different scenarios of sediment yield (fig. S11).

The lower Yellow River has been subject to intensive regulations during the era of imperial China. Many strategies have been proposed and practiced to tame the river, which can be summarized into two contrasting categories (43): "widening the channel to entrap sediments" versus "narrowing the channel by embankment to scour sediments." Our analyses suggest that embankment represents the least expedient strategy for flood control, which unfortunately has been practiced extensively in history. This "bottom-up" approach has only short-term effects on flood mitigation. Throughout the last millennium, imperial China witnessed a repetitive pattern of growth and collapse (35). At the beginning of each cycle, increased expenditure on levee networks under favorable political conditions provided the riparian communities with enough protection from flooding, thereby giving rise to a thriving agricultural economy. However, in the wake of each cycle, the levee networks struggled to withstand the increased financial pressure, which eventually transformed minor floods into devastating inundations and wrought chaos upon human societies. If the levee was not fixed timely after a breach, the flow would either excavate a new channel along a more favorable topographic gradient or capture a preexisting channel in a process known as avulsion. As sediment supply originating in the Loess Plateau continued to increase,
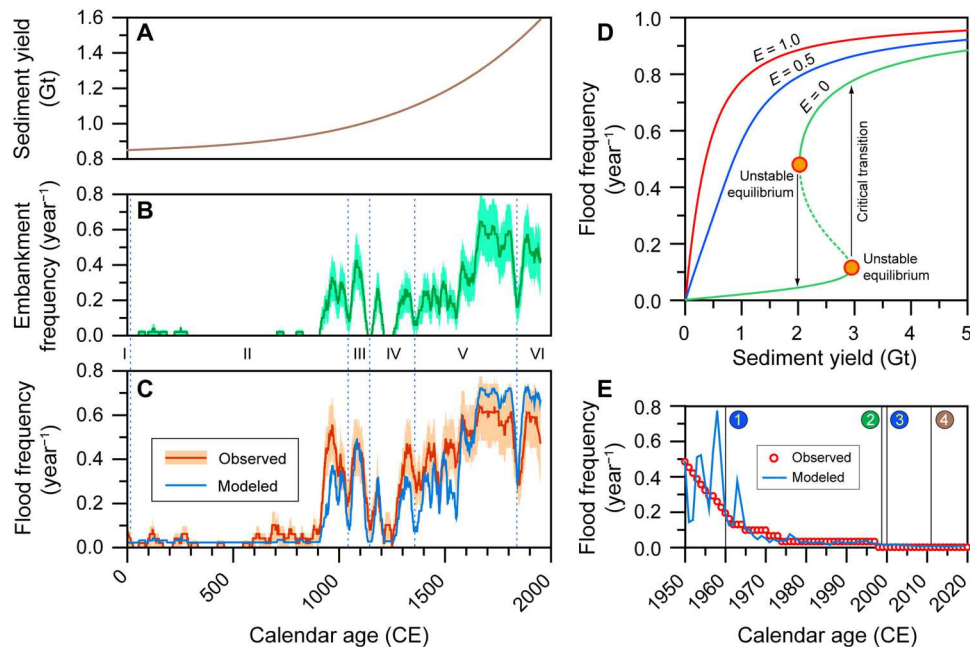
Fig. 4. Dynamics of Yellow River flood hazard in response to the enhancing human impacts on the river and its basin during the last two millennia. (**A**) Reconstructed annual sediment yield (*28*). (**B**) Embankment frequency in a 31-year overlapping moving window (*12, 13*). Major river stages are as follows: I, 602 BCE to 11 CE; II, 11 to 1048 CE; III, 1048 to 1128 CE; IV, 1128 to 1368 CE; V, 1368 to 1855 CE; and VI, 1855 CE to present. (**C**) Comparison of the observed with modeled flood frequency in a 31-year overlapping moving window. (**D**) Bifurcation diagrams showing the critical transition of flood frequency triggered by catchment erosion under three contrasting scenarios of embankment frequency. (**E**) Modeled flood frequency. Major river engineering and soil and water conservation projects: 1, completion of the Sanmenxia Dam; 2, commencement of the Grain for Green program; 3, completion of the Xiaolangdi Dam; and 4, initiation of the "Gully Land Consolidation" Project.

siltation started over in the new channel and embankment followed, thereby beginning the avulsion cycle anew.

On the basis of the analysis of operation of the fluvial system (fig. S10), we propose that proactive catchment management (e.g., soil and water conservation) represents a "top-down" approach to flood control. Comprehensive management of the Loess Plateau began in the 1950s, and currently, two soil and water conservation policies are in force (*44*). To assess the effect of positive human intervention in the river system on flood mitigation, we model flood frequency changes since 1950 CE driven by instrumental sediment load at the Tongguan station (representative of erosion over the Loess Plateau) and a persistent low embankment frequency (0.05 year^{-1}). Our result—as corroborated by observational data—indicates that flood frequency decreased progressively and flood hazard nearly vanished following the implementation of the "Grain for Green" program and the construction of the Xiaolangdi Dam (Fig. 4E).

Our main finding that flood frequency in the Yellow River basin has increased to an unprecedentedly high level over the last millennium, together with the results from the lower Mississippi River and elsewhere (*6–8*), suggests that enhanced human modifications to the river system have played a dominant role in elevating flood hazards in the backdrop of climate changes and thus urging the need to incorporate extensive catchment changes and widespread embankment into the prediction of flood hazards in major rivers of the world (*45*). Predictions ignoring future land-use changes may underestimate flood hazards, especially in densely populated regions where increasing demand for food supply and economic development could deteriorate their already highly erosive land use (*46*).

Meanwhile, we show that embankment, despite its short-term benefits, may boost long-term flood hazard through a suite of positive feedback loops. Therefore, structural flood control should be used together with other risk-mitigation strategies for long-term benefits (*47–49*). We also found that enforcing soil and water conservation policies is overwhelmingly important for flood hazard reduction. Nevertheless, attention still needs to be paid to extreme precipitation events in a warming climate, providing that atmospheric water-holding capacity is expected to increase exponentially with temperature and that heavy precipitation is positively correlated to atmospheric warming (*50*). Our results provide a knowledge base not only for the planning and design application of river engineering but also for developing deliverable adaptive strategies and preventive measures that may be readily transferable to other human-dominated rivers.

MATERIALS AND METHODS
Bayesian age modeling of paleo-flood events
The hierarchical framework provides a flexible approach through which our initial knowledge about the true ages of paleo-flood events and model parameters can be translated into prior information and integrated with the laboratory (observational) ages to yield a posterior estimate of the true flood event timeline with less uncertainty. The model was described as follows:

Let $\mathbf{X} = \{x_i \pm \epsilon_i | i = 1, 2, \cdots, M\}$ be a list of M laboratory ages of the paleo-flood events, each of which has a 1σ error, and $\mathbf{T} = \{t_i | i = 1, 2, \cdots, M\}$ be a list of M true ages of the paleo-flood events. Because of lack of knowledge, a weakly informative prior for the true ages is

used. Therefore, for the M laboratory ages, the corresponding true ages, say $\mathbf{T}$, are assumed to follow the uniform distribution supported on the interval of $[A, B]$ with a prior probability density function expressed as

$$f(\mathbf{T}|A, B) = \frac{1}{(|A - B|)^M} I(\mathbf{T}|A, B) \tag{1}$$

where A and B are two hyperparameters defining the early and late boundaries of the study period, respectively, and $I(\mathbf{T}|A, B)$ is an indicator function defined as

$$I(\mathbf{T}|A, B) = \begin{cases} 1 & \mathbf{T} \subseteq [A, B] \\ 0 & \mathbf{T} \supset [A, B] \end{cases} \tag{2}$$

Given the multisource nature, $\mathbf{X}$ can be split into two subsets: $\mathbf{X}_r = \{x_{rj} \pm \epsilon_{rj} | j = 1, 2, \cdots, M_r\}$ and $\mathbf{X}_o = \{x_{oj} \pm \epsilon_{oj} | j = 1, 2, \cdots, M_o\}$, denoting M_r laboratory radiocarbon ages and M_o laboratory OSL ages, respectively. Accordingly, we split $\mathbf{T}$ into two subsets: $\mathbf{T}_r = \{t_{rj} | j = 1, 2, \cdots, M_r\}$ and $\mathbf{T}_o = \{t_{oj} | j = 1, 2, \cdots, M_o\}$, corresponding to M_r true radiocarbon ages and M_o true OSL ages, respectively. For radiocarbon ages, a special treatment is required. Let $\mu \pm \theta$ denote the mean and the associated one-sigma error of a laboratory radiocarbon age in the calibration curve, which is a function of the true radiocarbon age. Therefore, given a true radiocarbon age, say t_{rj}, where $j = 1, 2, \cdots, M_r$, the corresponding laboratory radiocarbon age, say x_{rj}, is assumed to follow the normal distribution with a mean laboratory radiocarbon age in the calibration curve and an additive variance of the laboratory radiocarbon age and that in the calibration curve multiplied by a positive number [51]. Hence, the likelihood function can be expressed as

$$\mathcal{L}(\mathbf{X}_r|\mathbf{T}_r) = \prod_{j=1}^{M_r} \frac{1}{\sqrt{2\pi\delta[\epsilon_{rj}^2 + \theta^2(t_{rj})]}} \exp\left\{ -\frac{[x_{rj} - \mu(t_{rj})]^2}{2\delta[\epsilon_{rj}^2 + \theta^2(t_{rj})]} \right\} \tag{3}$$

where $\delta \in (0, +\infty)$ is a positive scale parameter. This property suggests that the Jeffreys prior can be used as the prior distribution of this parameter, leading to an improper probability density function expressed as

$$f(\delta) = \frac{1}{\delta} \tag{4}$$

Integrating out this parameter yields an integrated likelihood function for the radiocarbon ages [51, 52], which can be expressed as

$$\mathcal{L}(\mathbf{X}_r|\mathbf{T}_r) = \Gamma\left(\frac{M_r}{2}\right) \left\{ \sum_{j=1}^{M_r} \frac{[x_{rj} - \mu(t_{rj})]^2}{2[\epsilon_{rj}^2 + \theta^2(t_{rj})]} \right\}^{-\frac{M_r}{2}} \tag{5}$$

where $\Gamma(\cdot)$ denotes the gamma function. For OSL ages, given the true age, say t_{oj}, where $j = 1, 2, \cdots, M_o$, the corresponding laboratory age, say x_{oj}, is assumed to follow the normal distribution, leading to the likelihood function expressed as

$$\mathcal{L}(\mathbf{X}_o|\mathbf{T}_o) = \prod_{j=1}^{M_o} \frac{1}{\sqrt{2\pi}\epsilon_{oj}} \exp\left[-\frac{(x_{oj} - t_{oj})^2}{2\epsilon_{oj}^2} \right] \tag{6}$$

Making use of Bayes' theorem, the posterior probability density function of true ages, $\mathbf{T}$, can be readily expressed as

$$p(\mathbf{T}|\mathbf{X}) \propto \mathcal{L}(\mathbf{X}_r|\mathbf{T}_r) \times \mathcal{L}(\mathbf{X}_o|\mathbf{T}_o) \times f(\mathbf{T}|A, B) \tag{7}$$

This model framework was implemented using the MCMC method. We update the current state of $\mathbf{T}$ using a random walk process on the interval $[A, B]$ such that

$$\mathbf{T}^*|A, B = \mathbf{T} + \rho \times \mathbf{u} \tag{8}$$

where $\mathbf{u}$ denotes a vector of M random numbers drawn from the uniform distribution supported on $[-1, 1]$ and ρ is the step size of the random walk. The acceptance/rejection of the proposed move of the chain was determined according to the Metropolis-Hastings algorithm [53]. Note that the MCMC method is simulation-based, and several diagnostic analyses and treatments in terms of convergence, burn-in period, and thinning of the chain should be conducted. After a burn-in period of 2000 iterations, the chains were updated iteratively for 20,000 times and thinned out by keeping every 20th sample to remove the potential autocorrelation. The convergence of the chains was monitored using the method proposed by Gelman [54]. Specifically, we run three chains parallelly with different initial values. The ratio of the between-sequence to within-sequence variance in terms of the potential scale reduction factor, $\hat{R}$, was calculated. Upon convergence, we mix the three parallel chains with equal proportions, yielding 1000 uncorrelated timelines of paleo-flood events.

Kernel density estimation of flood occurrence rate

On the basis of Bayesian age modeling, we infer the true ages of paleo-flood events from the sedimentary records. A total of 1000 uncorrelated timelines of paleo-flood events were obtained using the MCMC method. The less error-prone historical and modern flood events were assumed to be independent and identically distributed observations instead of coming from a nonstationary Poisson point process [55]. Therefore, we bootstrap these flood events through random permutation with replacement for 1000 times as well to accommodate the propagation of error from the sedimentary record. These two sets of flood events were then combined by taking the union operation and removing duplicate ages, forming a suite of long time series of distinct flood events covering the Holocene.

Let $x_t = \sum_{i=1}^{N} \delta(t - t_i)$ denote a binary time series with N flood events occurring instantly at time t_i, where $i = 1, 2, \cdots, N$, $t \in [-10,000, 2000]$ is time in year BCE/CE, and $\delta(\cdot)$ denotes the Dirac delta function defined as

$$\delta(t - t_i) = \begin{cases} 1, & t = t_i \\ 0, & \text{otherwise} \end{cases} \tag{9}$$

The flood occurrence rate, $\lambda(t)$, can be estimated by convoluting the binary event time series, x_t, with a Gaussian kernel

$$\hat{\lambda}(t) = \frac{1}{N} \int_{-\infty}^{\infty} x_{t-\tau} \frac{1}{\sqrt{2\pi}h_t} \exp\left(-\frac{\tau^2}{2h_t^2} \right) d\tau \tag{10}$$

where h_t is the time-varying bandwidth. We estimate the locally adapted bandwidth by iteratively computing optimal fixed-size bandwidths within local intervals [56]. The fast Fourier

transformation method was used to speed up the computation. The mean, 70%, and 95% confidence intervals are calculated, thereby transferring the temporal uncertainty in the data into the equivalent error in the calculated flood frequency.

Correction for taphonomic bias

It has long been observed in palaeosciences—archaeology, paleontology, and geology—that the longer something is in existence, the more chances it has to be removed from the record by erosion, weathering, and/or bioturbation in a process collectively known as taphonomic loss, thereby causing overrepresentation of recent events relative to older ones (57). Such a taphonomic bias is generally referred to as the Sadler effect (58). Paleo-flood slack water deposits, upon accumulation, are subaerially exposed. With a loose structure, they are prone to erosion. Every successive flood with a peak stage capable of inundating previously accumulated slack water deposits may remove the sediments, causing a sedimentary hiatus. In addition, the thickness of slack water deposits and flood magnitude appear to be closely related (14). Thick slack water deposits are derived from large floods, and thus they are less erodible. Therefore, the sedimentary record of flood events is potentially incomplete, representing only large and/or extreme floods. The monotonically increasing pattern in the sedimentary record, if any, may be an artifact of taphonomic bias through time rather than a true representation of past events.

To test whether our sedimentary record is subject to the time-dependent taphonomic loss, we examine the frequency distribution of OSL and calibrated radiocarbon ages of paleo-flood slack water deposits following the approach proposed by Surovell and Brantingham (57). Specifically, we build up the empirical frequency distribution of paleo-flood events by counting the number of events in each 500-year interval between 10,000 BCE and 1950 CE. Our result shows that (i) there is a long-term general trend of decreasing flood frequency from 1300 BCE to 10,000 BCE, which may reflect taphonomic bias through time; (ii) there is a drop-off in flood frequency during the most recent time period from 1300 BCE onward, probably associated with research bias against recent paleo-flood slack water deposits; and (iii) there are short-term fluctuations in the flood frequency due likely to a product of both changes in flood activity and chance in sampling. These features are similar to those shown by the frequency distribution of radiocarbon ages of volcanic deposits (59), which have been proposed as a proxy for the temporal frequency distribution of terrestrial sediments globally.

Furthermore, we compare the frequency of ages of paleo-flood slack water deposits with that of volcanic deposits for the time period between 10,000 BCE and 1950 CE (59). A close correlation ($r = 0.82$ and $P < 0.001$) suggests that the empirical volcanic model of taphonomic bias can be applied on our sedimentary paleo-flood record (15). This model is based on a dataset of 2021 calibrated radiocarbon ages of global volcanic deposits (59), from which we derive a calibration curve for sedimentary records subject to taphonomic loss. The curve shows that the survival rate decreases exponentially as time elapses—half of paleo-flood slack water deposits will lose in about 1500 years, and only approximately 10% will remain in about 12,000 years.

Note that levee breaches and/or overtops, if occurred in less populated areas, may have not been observed and reported to the local and central governments. This is true particularly for early historical time. Similar to the sedimentary record, the earlier the levee breaches or overtops are in existence, the higher the likelihood that they have missed out on the chance to be documented in historical text. Therefore, the documentary record of historical flood events may be incomplete, which was also considered "taphonomic bias."

We correct our flood record for taphonomic bias by dividing the calculated flood occurrence rate by the survival rate for the time period between 10,000 BCE and 1950 CE. Both the taphonomically uncorrected and corrected records exhibit considerable variations superimposed on a monotonically increasing trend. Clearly, taphonomic loss has a remarkable impact on the result. For example, after taphonomic correction, flood occurrence rate was increased by an order of magnitude before 3000 BCE, while flood occurrence rate was only doubled from 3000 BCE to 500 CE. To evaluate the potential influence of taphonomic bias on the trend in our flood frequency record, we conduct Cox-Stuart test (60). Our results provide strong evidence ($P < 0.0001$) against the null hypothesis of trend absence in both the taphonomically uncorrected and corrected records at the 0.05 significance level.

Attribution analysis

To untangle the effects of human disturbances and natural factors, attribution of the observed increase in flood frequency during the last millennium was conducted using multiple linear regression analyses. We collect proxy records of climatic and environmental changes in the middle and lower Yellow River area during the last 12,000 years from the published literature. These records are considered natural drivers of the long-term variability in flood frequency, which include the following: (i) pollen-based quantitative reconstruction of annual precipitation from Lake Gonghai (18), a hydrologically closed alpine lake situated on the northeastern margin of the Chinese Loess Plateau. With limited human impacts, this lake is well suited for documenting natural climatic variability. Spatial correlation analyses of the instrumental data indicate that precipitation at this site represents much of North China, exhibiting a clear seasonality modulated by the East Asian summer monsoon. The fossil pollen data were transferred quantitatively to annual precipitation based on the modern pollen-climate relationship defined by a dataset consisting of 509 surface pollen samples along a large precipitation gradient and a small mean annual temperature gradient. The statistical model was well validated against instrumental data for the most recent period (1962 to 2008 CE). A close correlation suggests that the reconstruction is robust; (ii) relative abundance of coniferous tree pollen from the Sujiawan section on the western Chinese Loess Plateau (19). The landform of the Chinese Loess Plateau consists of three major types such as loess platforms, ridges, and hills essentially formed by erosion. These areas are usually colonized by grasses characterizing the arid/semi-arid zonal vegetation. Gullies represent areas subject to severe soil erosion and land degradation, which contribute 60 to 90% of the total sediment yield. If gully erosion ceases, coniferous trees would grow locally. Therefore, we interpret the coniferous tree pollen record from this site as an indicator of landscape stability in gully areas and (iii) frequency of soil development over the Loess Plateau (20). Paleosol development in the Chinese Loess Plateau has long been used as a direct and reliable proxy of the East Asian summer monsoon. Colloquially referred to as S_0, the black loam is a paleosol layer that commonly occurs close to the top of Holocene loess-paleosol sequences. This record is based on 229 radiocarbon

ages of black loam layers in 77 profiles across the Loess Plateau, which was interpreted as a proxy of the variations of the East Asian summer monsoon in this area.

While these records exhibit more or less coherent variations, PCA was conducted to extract common features from this dataset. PCA axis 1 explained 91% of the variance in the entire dataset. It is positively loaded by all factors, but mostly annual precipitation and vegetation cover. PCA axis 2 explained almost all of the remaining variance in the dataset. It is highly positively loaded by vegetation cover and soil development but negatively related to annual precipitation. In contrast, PCA axis 3 only explained a trivial amount (1%) of the variance, which is not worth interpreting. Therefore, the first two leading PCs, denoted as x_1 and x_2, were used to construct the regression model

$$\lambda = \beta_0 + \beta_1 x_1 + \beta_2 x_2 + \varepsilon \tag{11}$$

where β_0, β_1, and β_2 are parameters to be estimated using data of the baseline period and ε is error.

We define the baseline condition as a physical setting, with respect to which the natural variations of flood frequency in subsequent time periods are predicted and anthropogenic contributions are derived accordingly. The time period of 5000 to 2500 BCE was chosen as the baseline, because (i) the geomorphic boundary condition was similar to that of subsequent time periods. High-resolution sea-level record from the Bohai Bay shows that local sea level continued to rise from 10,000 BCE and reached the present-day position by about 5000 BCE (17), thereby turning the river channel from an incising to an aggrading system; and (ii) human impacts were minimal. This time period corresponds to the middle Neolithic, before the full establishment of millet-based agriculture and the widespread introduction of domesticates such as sheep/goat, cattle, and bread wheat characterizing the steppe cultural elements as well as technological innovations such as metallurgy and coal mining (21). In addition, archaeological data show that centralized, hierarchical settlement systems were not well developed in this area until 2500 BCE. Since then, the number of fortifications and site clustering began to increase, and early states were formed (21), pointing to the enhancement of human impacts from the late Neolithic onward.

We use data covering the baseline period (i.e., 5000 to 2500 BCE) to train the regression model. Once optimal model parameters were obtained, the model was used to generate predictions of natural variations in flood frequency for the last millennium. Last, the total and natural changes in flood frequency with respect to the baseline were calculated, respectively, and anthropogenic contributions are defined as the difference between the changes in total (observed) and predicted flood frequency. Our regression model was validated according to the coefficient of determination and the root mean square error, which were calculated to be 0.68 and 0.0077, respectively. The close similarity of the predicted to the observed flood frequency for the baseline period (5000 to 2500 BCE) further demonstrates the robustness of our regression model.

Modeling and bifurcation analysis of flood frequency
We calculate flood frequency during the CE using a sliding boxcar window with a bandwidth of 31 years and model the dynamics of flood hazard in a levee-lined channel system using a minimalistic one-dimensional ordinary differential equation

$$\frac{dF}{dt} = rF(1 - F) - \frac{bF^2}{a^2 + F^2} \tag{12}$$

where F is flood frequency varying between 0 and 1 year^{-1}, t is time in calendar years CE, r is the net rate of growth of the flood frequency, a is harvesting efficiency, and b is maximum harvesting rate. Two processes governing the change in the flood frequency were considered: One is intrinsic growth driven by channel aggradation, and the other is harvesting caused by river management. The former is modeled using a logistic function, while the latter is modeled using Holling's type III functional response.

Major human modifications to the fluvial system are twofold: One is soil erosion over the Loess Plateau, and the other is embankment on the lower Yellow River. We consider catchment erosion a slowly varying process that governs the intrinsic growth of flood frequency through channel aggradation. Therefore, r can be parameterized as $r = k_1 S(t)$, where $S(t)$ is the time-varying sediment yield consisting of the natural and anthropogenic components. According to Shi et al. (28), the anthropogenic components, $S_a(t)$, can be modeled using a power function

$$S_a(t) = 0.65 \left(\frac{t + 500}{2450} \right)^{4.4} \tag{13}$$

while the natural component, $S_n(t)$, can be modeled using a quadratic function

$$S_n(t) = 0.41 \left[0.00561 \left(\frac{1950 - t}{1000} \right)^2 - 0.123 \left(\frac{1950 - t}{1000} \right) + 2.29 \right] \tag{14}$$

We consider embankment a fast process that can readily accelerate flood frequency through raising the base flow in a confined channel. Therefore, a can be parameterized as $a = k_2 + k_3 E(t)$, where $E(t)$ is the time-varying embankment frequency calculated using the same method as for the flood frequency.

We optimize model parameters by minimizing the sum of squared difference between the modeled and observed flood frequencies. Once the optimal model parameters were obtained, we conduct bifurcation analysis to understand the regime shift of flood frequency by visualizing the system's equilibria and how their relationships change as a model parameter is varied. The bifurcation diagram and nonzero equilibria can be obtained by setting $dF/dt = 0$ in Eq. 12. Either S or E can be solved from $rF(1 - F) - \frac{bF^2}{a^2 + F^2}$ by keeping the other fixed.

REFERENCES AND NOTES
1. G. Blöschl, J. Hall, J. Parajka, R. A. P. Perdigão, B. Merz, B. Arheimer, G. T. Aronica, A. Bilibashi, O. Bonacci, M. Borga, I. Čanjevac, A. Castellarin, G. B. Chirico, P. Claps, K. Fiala, N. Frolova, L. Gorbachova, A. Gül, J. Hannaford, S. Harrigan, M. Kireeva, A. Kiss, T. R. Kjeldsen, S. Kohnová, J. J. Koskela, O. Ledvinka, N. Macdonald, M. Mavrova-

Guirguinova, L. Mediero, R. Merz, P. Molnar, A. Montanari, C. Murphy, M. Osuch, V. Ovcharuk, I. Radevski, M. Rogger, J. L. Salinas, E. Sauquet, M. Šraj, J. Szolgay, A. Viglione, E. Volpi, D. Wilson, K. Zaimi, N. Živković, Changing climate shifts timing of European floods. *Science* **357**, 588–590 (2017).

2. G. Blöschl, A. Kiss, A. Viglione, M. Barriendos, O. Böhm, R. Brázdil, D. Coeur, G. Demarée, M. C. Llasat, N. Macdonald, D. Retsö, L. Roald, P. Schmocker-Fackel, I. Amorim, M. Bělínová, G. Benito, C. Bertolin, D. Camuffo, D. Cornel, R. Doktor, L. Elleder, S. Enzi, J. C. Garcia, R. Glaser, J. Hall, K. Haslinger, M. Hofstätter, J. Komma, D. Limanówka, D. Lun, A. Panin, J. Parajka, H. Petrić, F. S. Rodrigo, C. Rohr, J. Schönbein, L. Schulte, L. P. Silva, W. H. J. Too- nen, P. Valent, J. Waser, O. Wetter, Current European flood-rich period exceptional compared with past 500 years. *Nature* **583**, 560–566 (2020).

3. H. C. Winsemius, J. C. J. H. Aerts, L. P. H. van Beek, M. F. P. Bierkens, A. Bouwman, B. Jongman, J. C. J. Kwadijk, W. Ligtvoet, P. L. Lucas, D. P. van Vuuren, P. J. Ward, Global drivers of future river flood risk. *Nat. Clim. Change* **6**, 381–385 (2016).

4. B. Tellman, J. A. Sullivan, C. Kuhn, A. J. Kettner, C. S. Doyle, G. R. Brakenridge, T. A. Erickson, D. A. Slayback, Satellite imaging reveals increased proportion of population exposed to floods. *Nature* **596**, 80–86 (2021).

5. J. Best, Anthropogenic stresses on the world's big rivers. *Nat. Geosci.* **12**, 7–21 (2019).

6. R. E. Criss, E. L. Shock, Flood enhancement through flood control. *Geology* **29**, 875–878 (2001).

7. N. Pinter, R. R. van der Ploeg, P. Schweigert, G. Hoefer, Flood magnification on the River Rhine. *Hydrol. Process.* **20**, 147–164 (2006).

8. S. E. Munoz, L. Giosan, M. D. Therrell, J. W. F. Remo, Z. Shen, R. M. Sullivan, C. Wiman, M. O'Donnell, J. P. Donnelly, Climatic control of Mississippi River flood hazard amplified by river engineering. *Nature* **556**, 95–98 (2018).

9. R. Mostern, Sediment and state in Imperial China: The Yellow River watershed as an earth system and a world system. *Nature and Culture* **11**, 121–147 (2016).

10. Y. Chen, J. P. Syvitski, S. Gao, I. Overeem, A. J. Kettner, Socio-economic impacts on flooding: A 4000-year history of the Yellow River, China. *Ambio* **41**, 682–698 (2012).

11. W.-J. Li, S.-Y. Yu, J. Pan, X. Cao, Y. Chen, Y. Wang, A 2000-year documentary record of levee breaches on the lower Yellow River and their relationship with climate changes and human activities. *Holocene* **31**, 333–345 (2021).

12. Y. Shen, S. Zhao, D. Zheng, *The Chronicle of the Yellow River* (Military Committee and Resources Committee of the Republic of China, 1935), pp. 216.

13. Yellow River Conservancy Commission, *The Chronicle of Events of the Yellow River* (Yellow River Water Conservancy Publishing House, 2001).

14. R. C. Kochel, V. R. Baker, Paleoflood hydrology. *Science* **215**, 353–361 (1982).

15. T. A. Surovell, J. B. Finley, G. M. Smith, P. J. Brantingham, R. Kelly, Correcting temporal frequency distributions for taphonomic bias. *J. Archaeol. Sci.* **36**, 1715–1724 (2009).

16. B. Fu, S. Wang, Y. Liu, J. Liu, W. Liang, C. Miao, Hydrogeomorphic ecosystem responses to natural and anthropogenic changes in the Loess Plateau of China. *Annu. Rev. Earth Planet. Sci.* **45**, 223–243 (2017).

17. J. Li, Z. Shang, F. Wang, Y. Chen, L. Tian, X. Jiang, H. Wang, Holocene sea level change on the west coast of the Bohai Bay. *Quaternary Sciences (in Chinese with English abstract)* **35**, 243–264 (2015).

18. F. Chen, Q. Xu, J. Chen, H. J. B. Birks, J. Liu, S. Zhang, L. Jin, C. An, R. J. Telford, X. Cao, Z. Wang, X. Zhang, K. Selvaraj, H. Lu, Y. Li, Z. Zheng, H. Wang, A. Zhou, G. Dong, J. Zhang, X. Huang, J. Bloemendal, Z. Rao, East Asian summer monsoon precipitation variability since the last deglaciation. *Sci. Rep.* **5**, 11186 (2015).

19. C.-B. An, Z.-D. Feng, L. Barton, Dry or humid? Mid-Holocene humidity changes in arid and semi-arid China. *Quat. Sci. Rev.* **25**, 351–361 (2006).

20. H. Wang, J. Chen, X. Zhang, F. Chen, Palaeosol development in the Chinese Loess Plateau as an indicator of the strength of the East Asian summer monsoon: Evidence for a mid- Holocene maximum. *Quat. Int.* **334-335**, 155–164 (2014).

21. C. Leipe, T. Long, E. Sergusheva, M. Wagner, P. Tarasov, Discontinuous spread of millet agriculture in eastern Asia and prehistoric population dynamics. *Sci. Adv.* **5**, eaax6225 (2019).

22. T. Long, C. Leipe, G. Jin, M. Wagner, R. Guo, O. Schröder, P. E. Tarasov, The early history of wheat in China from ^{14}C dating and Bayesian chronological modelling. *Nat. Plants* **4**, 272–279 (2018).

23. S.-Y. Yu, X. Chen, X. Liu, Z. Fang, J. Guo, S. Zhan, H. Fang, F. Chen, Ancient water wells reveal a prolonged drought in the lower Yellow River area about 2800 years ago. *Sci. Bull.* **63**, 1324–1327 (2018).

24. J. Dodson, X. Li, N. Sun, P. Atahan, X. Zhou, H. Liu, K. Zhao, S. Hu, Z. Yang, Use of coal in the Bronze Age in China. *Holocene* **24**, 525–530 (2014).

25. K. Chen, S. Liu, Y. Li, J. Mei, A. Shao, L. Yue, Evidence of arsenical copper smelting in Bronze Age China: A study of metallurgical slag from the Laoniupo site, central Shaanxi. *J. Archaeol. Sci.* **82**, 31–39 (2017).

26. W. Lam, J. Chen, J. Chong, X. Lei, W. L. Tam, An iron production and exchange system at the center of the Western Han Empire: Scientific study of iron products and manufac- turing remains from the Taicheng site complex. *J. Archaeol. Sci.* **100**, 88–101 (2018).

27. T. Kidder, H. Liu, Q. Xu, M. Li, The alluvial geoarchaeology of the Sanyangzhuang site on the Yellow River floodplain, Henan Province, China. *Geoarchaeology* **27**, 324–343 (2012).

28. C. Shi, Z. Dian, L. You, Changes in sediment yield of the Yellow River basin of China during the Holocene. *Geomorphology* **46**, 267–283 (2002).

29. J. Xu, Naturally and anthropogenically accelerated sedimentation in the lower Yellow River, China, over the past 13,000 years. *Geogr. Ann. Ser. B* **80**, 67–78 (1998).

30. M.-E. Ren, X. Zhu, Anthropogenic influences on changes in the sediment load of the Yellow River, China, during the Holocene. *Holocene* **4**, 314–320 (1994).

31. T. R. Kidder, Y. Zhuang, Anthropocene archaeology of the Yellow River, China, 5000–2000 BP. *Holocene* **25**, 1627–1639 (2015).

32. C.-C. Huang, J. Pang, X. Zha, H. Su, Y. Jia, Extraordinary floods related to the climatic event at 4200 a BP on the Qishuihe River, middle reaches of the Yellow River, China. *Quat. Sci. Rev.* **30**, 460–468 (2011).

33. S.-Y. Yu, Z. Hou, X. Chen, Y. Wang, Y. Song, M. Gao, J. Pan, M. Sun, H. Fang, J. Han, T. R. Kidder, F. H. Chen, Extreme flooding of the lower Yellow River near the Northgrip- pian-Meghalayan boundary: Evidence from the Shilipu archaeological site in south- western Shandong Province, China. *Geomorphology* **350**, 106878 (2020).

34. L. Xie, Z. Daudjee, C. F. Liu, P. Sebillaud, Settlement relocation, urban construction, and social transformation in China's Central Plain, 2300–1500 B.C. *Asian Perspect.* **59**, 299–329 (2020).

35. T. Wright, An economic cycle in imperial China? Revisiting Robert Hartwell on iron and coal. *J. Econ. Soc. Hist.* **50**, 398–423 (2007).

36. S. Zhu, in *Natural Environment and Evolution of the Loess Plateau of China*, Q. Yang, Ed. (Science Press, 1991), pp. 108–143.

37. K. Zhang, Y. Zhao, A. Zhou, H. Sun, Late Holocene vegetation dynamic and human ac- tivities reconstructed from lake records in western Loess Plateau, China. *Quat. Int.* **227**, 38–45 (2010).

38. C. Zhang, C. Zhao, A. Zhou, K. Zhang, R. Wang, J. Shen, Late Holocene lacustrine envi- ronmental and ecological changes caused by anthropogenic activities in the Chinese Loess Plateau. *Quat. Sci. Rev.* **203**, 266–277 (2019).

39. X. Wu, Y. Wei, B. Fu, S. Wang, Y. Zhao, E. F. Moran, Evolution and effects of the social- ecological system over a millennium in China's Loess Plateau. *Sci. Adv.* **6**, eabc0276 (2020).

40. N. Pinter, A. A. Jemberie, J. W. Remo, R. A. Heine, B. S. Ickes, Flood trends and river en- gineering on the Mississippi River system. *Geophys. Res. Lett.* **35**, L23404 (2008).

41. T. R. Kidder, H. Liu, Bridging theoretical gaps in geoarchaeology: Archaeology, geo- archaeology, and history in the Yellow River valley, China. *Archaeol. Anthropol. Sci.* **9**, 1585–1602 (2017).

42. S. Song, S. Wang, B. Fu, Y. Liu, K. Wang, Y. Li, Y. Wang, Sediment transport under increasing anthropogenic stress: Regime shifts within the Yellow River, China. *Ambio* **49**, 2015–2025 (2020).

43. Z. Wang, C. Liu, Two-thousand years of debates and practices of Yellow River training strategies. *Int. J. Sediment Res.* **34**, 73–83 (2019).

44. Y. Li, G. Du, Y. Liu, Transforming the Loess Plateau of China. *Front. Agri. Sci. Eng.* **3**, 181–185 (2016).

45. G. Grill, B. Lehner, M. Thieme, B. Geenen, D. Tickner, F. Antonelli, S. Babu, P. Borrelli, L. Cheng, H. Crochetiere, H. Ehalt Macedo, R. Filgueiras, M. Goichot, J. Higgins, Z. Hogan, B. Lip, M. E. McClain, J. Meng, M. Mulligan, C. Nilsson, J. D. Olden, J. J. Opperman, P. Petry, C. Reidy Liermann, L. Sáenz, S. Salinas-Rodríguez, P. Schelle, R. J. P. Schmitt, J. Snider, F. Tan, K. Tockner, P. H. Valdujo, A. van Soesbergen, C. Zarfl, Mapping the world's free- flowing rivers. *Nature* **569**, 215–221 (2019).

46. P. Borrelli, D. A. Robinson, L. R. Fleischer, E. Lugato, C. Ballabio, C. Alewell, K. Meusburger, S. Modugno, B. Schütt, V. Ferro, V. Bagarello, K. Van Oost, L. Montanarella, P. Panagos, An assessment of the global impact of 21st century land use change on soil erosion. *Nat. Commun.* **8**, 1–13 (2017).

47. G. Di Baldassarre, H. Kreibich, S. Vorogushyn, J. Aerts, K. Arnbjerg-Nielsen, M. Barendrecht, P. Bates, M. Borga, W. Botzen, P. Bubeck, B. De Marchi, C. Llasat, M. Mazzoleni, D. Molinari, E. Mondino, J. Märd, O. Petrucci, A. Scolobig, A. Viglione, P. J. Ward, Hess opinions: An interdisciplinary research agenda to explore the unintended consequences of structural flood protection. *Hydrol. Earth Sys. Sci.* **22**, 5629–5637 (2018).

48. N. S. Hutton, G. A. Tobin, B. E. Montz, The levee effect revisited: Processes and policies enabling development in Yuba County, California. *J. Flood Risk Manag.* **12**, e12469 (2019).

49. R. Collenteur, H. De Moel, B. Jongman, G. Di Baldassarre, The failed-levee effect: Do so- cieties learn from flood disasters? *Nat. Hazards* **76**, 373–388 (2015).

50. R. P. Allan, B. J. Soden, Atmospheric warming and the amplification of precipitation extremes. *Science* **321**, 1481–1484 (2008).

51. J. A. Christen, S. Pérez, A new robust statistical model for radiocarbon data. *Radiocarbon* **51**, 1047–1059 (2009).

52. S.-Y. Yu, MatCalib: A Matlab software package for Bayesian modeling of radiocarbon ages subject to temporal order constraints. *AIMS Geosci.* **8**, 16–32 (2022).

53. W. K. Hastings, Monte Carlo sampling methods using Markov chains and their applications. *Biometrika* **57**, 97–109 (1970).

54. A. Gelman, in *Markov Chain Monte Carlo in Practice*, W. R. Gilks, S. Richarson, D. J. Spiegelhalter, Eds. (Chapman and Hall, 1995), pp. 1–14.

55. A. Cowling, P. Hall, M. J. Phillips, Bootstrap confidence regions for the intensity of a Poisson point process. *J. Am. Stat. Assoc.* **91**, 1516–1524 (1996).

56. H. Shimazaki, S. Shinomoto, Kernel bandwidth optimization in spike rate estimation. *J. Comput. Neurosci.* **29**, 171–182 (2010).

57. T. A. Surovell, P. J. Brantingham, A note on the use of temporal frequency distributions in studies of prehistoric demography. *J. Archaeol. Sci.* **34**, 1868–1877 (2007).

58. P. M. Sadler, Sediment accumulation rates and the completeness of stratigraphic sections. *J. Geol.* **89**, 569–584 (1981).

59. R. U. Bryson, R. A. Bryson, A. Ruter, A calibrated radiocarbon database of Late Quaternary volcanic eruptions. *eEarth Discussions* **1**, 123–134 (2006).

60. A. Rutkowska, Properties of the Cox-Stuart test for trend in application to hydrological series: The simulation study. *Commun. Stat. Simul. Comput.* **44**, 565–579 (2015).

61. Yellow River Conservancy Commission, *Summary History of Yellow River Water Conservancy* (Water Conservancy and Electric Power Press, 1984).

62. J. Dai, *Encyclopedic Dictionary of Ancient and Modern Chinese Geographical Names* (Shanghai Lexicographical Publishing House, 2005).

63. Q. Tan, *The Historical Atlas of China* (Cartographic Publishing House, 1982).

64. P. C. Patton, V. R. Baker, R. C. Kochel, in *Adjustments of the Fluvial System,* D. D. Rhodes, G. P. Williams, Eds. (Routledge, 1979), pp. 225–253.

65. P. Zhang, J. Yang, H. Zhao, Z. Liu, L. Song, R. Zhang, W. Cao, Research progress of the Holocene paleoflood in the Yellow River basin and a future prospect. *Mar. Geol. Quat. Geology* **40**, 178–188 (2020).

66. Z. He, H. Long, L. Yang, J. Zhou, Luminescence dating of a fluvial sequence using different grain size fractions and implications on Holocene flooding activities in Weihe Basin, central China. *Quater. Geochronol.* **49**, 123–130 (2019).

67. W. Liu, C.-C. Huang, J. Pang, X. Zha, X. Zhao, G. Hu, B. Shi, Study on provenance of Holocene flood slackwater deposits in the Liulintan reach of the Yellow River. *Journal of Soil and Water Conservation* **30**, 136–142 (in Chinese with English abstract) (2016).

68. X. Li, C.-C. Huang, J. Pang, Palaeoflood events in the lower reaches of the Wudinghe River. *Arid Land Geography* **43**, 380–387 (in Chinese with English abstract) (2020).

69. L. Fan, C.-C. Huang, J. Pang, X. Zha, Y. Zhou, X. Li, T. Liu, Sedimentary records of palaeofloods in the Wubu reach along the Jin-Shaan gorges of the middle Yellow River, China. *Quat. Int.* **380**, 368–376 (2015).

70. C.-C. Huang, X. Li, J. Pang, X. Zha, Y. Zhou, Palaeoflood sedimentological and hydrological studies on the Yongheguan reach in the middle Yellow River. *Acta Geographica Sinica* **67**, 1494–1504 (2012).

71. W. Liu, C.-C. Huang, J. Pang, X. Zhao, Y. Zhou, B. Shi, Holocene palaeoflood and climatic changes at the Matouguan Reach of the Yellow River. *Arid Land Geography*, 85–93 (2017).

72. T. Liu, C.-C. Huang, J. Pang, Y. Zhou, Y. Zhang, L. Ji, R. Shang, Extraordinary hydro-climatic events during 1800–1600 yr BP in the Jin-Shaan Gorges along the middle Yellow River, China. *Palaeogeogr. Palaeoclimatol. Palaeoecol.* **410**, 143–152 (2014).

73. X. Li, C.-C. Huang, J. Pang, X. Zha, G. Hao, B. Ge, Hydrological studies of the Holocene palaeoflood in the Hukou reach of the Yellow River. *Acta Geographica Sinica* **65**, 1371–1380 (2010).

74. Y. Ma, C.-C. Huang, Y. Zhou, J. Pang, X. Zha, X. Li, OSL dating of the Holocene paleoflood events in the Jixian reach along the middle Yellow River. *Quat. Sci.* **34**, 372–380 (2014).

75. Y. Li, C.-C. Huang, H. H. Ngo, S. Yin, Z. Dong, Y. Zhang, Y. Chen, Y. Lu, W. Guo, Analysis of event stratigraphy and hydrological reconstruction of low-frequency flooding: A case study on the Fenhe River, China. *J. Hydrol.* **603**, 127083 (2021).

76. B. Shi, C.-C. Huang, J. Pang, X. Zha, Palaeoflood events and climate change at the turning time from the Shang to Zhou Dynasty in the Longmen reach of the Yellow River. *J. Lake Sci.* **29**, 234–245 (2017).

77. Y. Guo, "Study on paleoflood hydrology of several rivers in Chinese monsoon region on a scale of 10,000 years," thesis, Shaanxi Normal University, Xi'an (2017).

78. Y. Guo, C.-C. Huang, J. Pang, Y. Zhou, X. Zha, P. Mao, Reconstruction palaeoflood hydrology using slackwater flow depth method in the Yanhe River valley, middle Yellow River basin, China. *J. Hydrol.* **544**, 156–171 (2017).

79. G. Hao, "The study of Holocene paleoflood hydrology from Wubao to Yanchang in the middle reach of the Yellow River," thesis, Shaanxi Normal University, Xi'an (2013).

80. Y. Zhang, C.-C. Huang, J. Pang, X. Zha, Y. Zhou, X. Wang, Holocene palaeoflood events recorded by slackwater deposits along the middle Beiluohe River valley, middle Yellow River basin, China. *Boreas* **44**, 127–138 (2015).

81. X. Wang, C.-C. Huang, J. Pang, X. Zha, Y. Zhou, H. Wang, H. Gu, L. Zhou, H. Wei, Holocene palaeo-floods and climatic changes in the Yijun reaches of the Beiluohe River, middle reaches of the Yellow River. *J. Lake Sci.* **23**, 910–918 (2011).

82. Y. Li, C.-C. Huang, H. H. Ngo, J. Pang, X. Zha, T. Liu, W. Guo, In situ reconstruction of long-term extreme flooding magnitudes and frequencies based on geological archives. *Sci. Total Environ.* **670**, 8–17 (2019).

83. B. Shi, C.-C. Huang, J. Pang, X. Zha, T. Liu, W. Liu, Hydrological reconstruction of the Holocene palaeoflood in the Tianshui east reach of the upper Weihe River. *Arid Land Geography*, 573–581 (in Chinese with English abstract) (2016).

84. H. Wang, C.-C. Huang, Y. Zhou, J. Pang, X. Zha, H. Gu, L. Zhou, OSL dating of the Holocene paleoflood events on the Qianhe River in the Guanzhong Basin, China. *Scientia Sinica Terrae* **42**, 390–401 (in Chinese with English abstract) (2012).

85. C.-C. Huang, J. Pang, X. Zha, Y. Zhou, Prehistorical floods in the Guanzhong Basin in the Yellow River drainage area: A case study along the Qishuihe River Valley over the Zhouyuan Loess Tableland. *Scientia Sinica Terrae* **41**, 1658–1669 (in Chinese with English abstract) (2011).

86. X. Zha, C.-C. Huang, J. Pang, Holocene extreme floods and environmental change of Qishuihe River in western Guanzhong Basin. *Acta Geogr. Sin.* **62**, 291–300 (2007).

87. H. Wan, C.-C. Huang, B. Ge, J. Pang, Hydrological reconstruction of Holocene paleofloods in Baoji-Tianshui gorge, upper Weihe River basin, China. *Quat. Int.* **521**, 138–146 (2019).

88. H. Wang, C.-C. Huang, Y. Zhou, J. Pang, X. Zha, H. Gu, OSL dating of the palaeoflood events in the middle reaches of the Weihe River. *Acta Sedimentologica Sinica* **30**, 346–355 (in Chinese with English abstract) (2012).

89. C.-C. Huang, J. Pang, X. Zha, Y. Zhou, H. Su, Y. Li, Extraordinary floods of 4100–4000 a BP recorded at the Late Neolithic ruins in the Jinghe River gorges, Middle Reach of the Yellow River, China. *Palaeogeogr. Palaeoclimatol. Palaeoecol.* **289**, 1–9 (2010).

90. H. Gu, C.-C. Huang, Y. Zhou, J. Pang, X. Zha, Y. Zhang, OSL dating study on the palaeoflood events recorded in the Yangguanzhai Neolithic ruins in the Guanzhong Basin. *Geogr. Res.* **31**, 1837–1848 (2012).

91. J. Wang, C.-C. Huang, J. Pang, X. Zha, Y. Zhou, Y. Zhang, Holocene paleofloods slackwater deposit in lower reaches of Weihe River. *Bull. Soil Water Conserv.* **31**, 32–37 (2011).

92. H. Wang, C.-C. Huang, Y. Zhou, J. Pang, X. Zha, H. Gu, OSL dating of the Holocene paleoflood events: A case study of the Lintong segment in the lower Weihe River valley. *Acta Geoscientica Sinica* **33**, 227–235 (in Chinese with English abstract) (2012).

93. C.-C. Huang, J. Pang, X. Zha, H. Su, Y. Jia, Y. Zhu, Impact of monsoonal climatic change on Holocene overbank flooding along Sushui River, middle reach of the Yellow River, China. *Quat. Sci. Rev.* **26**, 2247–2264 (2007).

94. Y. Zhang, C.-C. Huang, Z. Tan, Y. Chen, H. Qiu, C. Huang, Y. Li, Y. Zhang, X. Li, J. Shulmeister, N. Patton, L. Liu, Y. Zhu, N. Wang, Prehistoric and historic overbank floods in the Luoyang Basin along the Luohe River, middle Yellow River basin, China. *Quat. Int.* **521**, 118–128 (2019).

95. X. Zhao, C.-C. Huang, J. Pang, X. Zha, Y. Guo, G. Hu, Holocene climatic events recorded in palaeoflood slackwater deposits along the middle Yiluohe River valley, middle Yellow River basin, China. *J. Asian Earth Sci.* **123**, 85–94 (2016).

96. G. Hu, C.-C. Huang, Y. Zhou, J. Pang, X. Zha, Y. Guo, Y. Zhang, X. Zhao, Hydrological studies of the historical and palaeoflood events on the middle Yihe River, China. *Geomorphology* **274**, 152–161 (2016).

97. J. Zhang, Z. Xia, Deposition evidences of the 4 ka BP flood events in Central China Plains. *Acta Geographica Sinica* **66**, 685–697 (in Chinese with English abstract) (2011).

98. M. Yang, S. Wang, S. Kang, H. Li, X. Wang, Optically stimulated luminescence dating of Sanyangzhuang profile, Henan Province. *Journal of Earth Environment* **9**, 580–588 (in Chinese with English abstract) (2019).

99. Y. Li, "Late-Holocene paleoflood records in the ancient Daluze area of the Hebei Plain," thesis, China University of Geosciences, Beijing (2016).

100. Z. Ge, D. Yang, Y. Xie, X. Li, Holocene extraordinary flood of Qinhe River and its recurrence interval. *Journal of Natural Disaster* **13**, 144–148 (in Chinese with English abstract) (2004).

101. D. Yang, G. Yu, Y. Xie, D. Zhan, Z. Li, Sedimentary records of large Holocene floods from the middle reaches of the Yellow River, China. *Geomorphology* **33**, 73–88 (2000).

102. P. Fu, "Design flood calculation of the Qin River based on paleoflood method," thesis, Hohai University, Nanjing (2005).